Materials Today Bio 28 (2024) 101230

Contents lists available at ScienceDirect

Materials Today Bio

journal homepage: www.journals.elsevier.com/materials-today-bio

Rhodium nanozyme mitigates RPE degeneration and preserves vision in age-related macular degeneration via antioxidant and anti-inflammatory mechanisms

Qian Sun [a], Yueqi Ni [a], Kang Wang [b], Hong Zhang [a], Jia Liu [c,**], Lingjuan Xu [a,***], Yin Zhao [a,*]

[a] Department of Ophthalmology, Tongji Hospital, Tongji Medical College, Huazhong University of Science and Technology, Wuhan, 430030, China
[b] Hubei Province Tobacco Quality Supervision and Test Station, Wuhan, 430030, China
[c] Research Center for Tissue Engineering and Regenerative Medicine, Union Hospital, Tongji Medical College, Huazhong University of Science and Technology, Wuhan, 430022, China

ARTICLE INFO

Keywords:
Nanozyme
RPE
Microglia
Oxidative stress
Inflammation

ABSTRACT

Age-related macular degeneration (AMD) is the leading cause of blindness among elderly people worldwide. However, there are currently no effective treatments for AMD. Oxidative stress-induced retinal pigment epithelium (RPE) degeneration and the inflammatory response are the main causes of AMD. In this study, a polyethylene glycol (PEG)-coated rhodium nanozyme (PEG-RhZ) with excellent reactive oxygen species (ROS) and reactive nitrogen species (RNS) elimination capability was synthesized for the treatment of AMD. PEG-RhZs protected RPE cell viability and barrier function upon exposure to oxidative stress stimuli. Additionally, microglial migration and iNOS, IL-1β and TNF-α expression were inhibited by PEG-RhZs. In the acute phase of the AMD model, PEG-RhZs significantly alleviated RPE oxidative damage and inhibited microglial activation. In the late stage of the AMD model, PEG-RhZs reduced photoreceptor loss and improved vision impairment. Furthermore, PEG-RhZs showed good biocompatibility and stability both *in vitro* and *in vivo*. Collectively, our findings suggest the therapeutic potential of PEG-RhZs for AMD treatment.

STATEMENT OF SIGNIFICANCE: AMD is a kind of retinal degenerative disease that poses heavy health burden globally. PEG-RhZs exhibiting robust ROS and RNS scavenging capabilities have shown promise in safeguarding retinal pigment epithelium (RPE) from oxidative stress, suppressing microglia activation and the secretion of pro-inflammatory molecules, mitigating loss of retinal photoreceptor cells, and ameliorating visual impairment. The commendable antioxidant properties, biological safety, and biostability of PEG-RhZs offer valuable insights for the clinical management of AMD.

1. Introduction

Age-related macular degeneration (AMD) is the leading cause of blindness among elderly individuals. Over 8.7 % of the worldwide population has AMD, and the number of patients is expected to increase; by 2040, the number of patients may reach 288 million [1,2]. As a sight-threatening disease, AMD seriously affects people's lives and places a heavy economic burden on society. The etiology of AMD is complex and includes genetic, environmental, and lifestyle factors. Numerous studies have shown that oxidative stress-induced RPE degeneration plays a central role in AMD initiation [3–5]. RPE cells interact with photoreceptors, Bruch's membrane, and choroidal capillaries. Due to its special location, the RPE phagocytoses photoreceptor outer segments, provides nutrition for photoreceptors and forms a part of the outer retinal blood barrier [1,3]. Photooxidative stress, pathological mitochondria, and compromised electron transport chain (ETC) components lead to reactive oxygen species (ROS) overproduction and RPE oxidative damage [3]. In addition, excessive ROS and oxidized lipoproteins activate the innate immune response in the retina of AMD patients. The recruitment of innate immune cells, such as microglia, causes retinal inflammation and the degeneration of photoreceptors [3,6,7]. In Ccr2-deficient mice, AMD-like degeneration induced by the lipid

** Corresponding author.
*** Corresponding author.
* Corresponding author.
E-mail addresses: jialiu1207@hust.edu.cn (J. Liu), xljuan@hust.edu.cn (L. Xu), zhaoyin85@hust.edu.cn (Y. Zhao).

https://doi.org/10.1016/j.mtbio.2024.101230
Received 6 May 2024; Received in revised form 17 August 2024; Accepted 3 September 2024
Available online 4 September 2024

peroxidation product carboxyethylpyrrole (CEP) can be alleviated, suggesting a deleterious role for these immune cells [8]. Moreover, in inflammation-prone Cx3cr1$^{GFP/GFP}$ mice, mononuclear cell-derived IL-1 leads to severe photoreceptor degeneration [9].

According to their clinical features, AMD can be classified as dry or wet [1]. Dry AMD, also known as geographic atrophy (GA), is characterized by progressing atrophy of the macula, whereas wet AMD or exudative AMD is related to choroidal neovascularization in the macula [1,4]. Dry AMD accounts for approximately 90 % of AMD patients, and this state can progress to wet AMD, leading to more severe vision loss. Although anti-VEGF drugs have been shown to delay the progression of wet AMD, there are currently no clinically approved therapies available to treat the more prevalent dry form [4]. Several genetic or other animal models have been developed to further understand the molecular pathobiology of dry AMD and to develop better therapies [7,10,11]. Sodium iodate (NaIO3) injection selectively induces RPE damage even when administered systemically, causing acute RPE cell death followed by a period of retinal inflammation and photoreceptor apoptosis, and outer retinal thinning is a widely used model of dry AMD [10,12]. Potential therapeutic candidates, such as carotenoids, polysaccharides, flavonoids, vitamins, and resveratrol, have been tested in preclinical and clinical dry AMD studies [5,13]. Some of these compounds have been shown to alleviate oxidative stress, counteract inflammation, and relieve the symptoms of AMD [5]. However, their clinical use is still limited by their poor bioavailability, short biological half-life, and other pharmacokinetic/pharmacodynamic challenges [4,5,13]. Therefore, there is an urgent need for new strategies to intervene in and treat dry AMD.

In recent years, nanomaterials with enzyme catalytic properties (nanozymes) with potent efficiency at low doses, high stability under different conditions, and good biosafety have been widely used in the biomedical field [14,15]. Nanozymes can scavenge overexpressed ROS in cells and inhibit inflammation [16]. Nanoceria can switch between Ce^{3+} and Ce^{4+} and mimic the nature of antioxidant enzymes [17]. In light-damaged rat retina models, cerium oxide nanoparticles can decrease the intracellular concentrations of ROS, protect photoreceptor cells, reduce microglial activation, and prevent loss of vision due to light-induced degeneration of photoreceptor cells [17,18]. However, the potential toxicity of these nanozymes is considered to be a barrier to the clinical treatment of retinal degenerative disease [19]. Noble metal rhodium nanozymes (RhZs) with high chemical stability, adaptable electronic space, and strong potential to mimic the catalytic activity of natural enzymes and reduce oxidative stress have attracted the interest of researchers [20,21]. RhZ has high catalytic activity, mimicking superoxide dismutase (SOD) and catalase (CAT), which can quench H_2O_2, O_2^-, and OH^- to protect cells from oxidative damage [20]. Additionally, the cyclometalated rhodium (III) complex blocks NLRP3 inflammasome activity in macrophages and alleviates inflammatory bowel disease [22]. In dextran sulfate sodium-induced colitis, RhZs scavenge RONS, decrease the levels of proinflammatory cytokines (TNF-α and IL-6) at inflammatory sites, and promote regeneration of the colonic epithelium [21]. The addition of polyethylene glycol (PEG) to RhZs further enhances their tissue penetration and retention, which allows for better distribution and longer-lasting protection [19,21]. Based on the direct antioxidant activity, anti-inflammatory effects, and good biocompatibility of PEG-RhZ, we hypothesized that it could be a potential treatment for AMD.

Herein, we used *in vitro* and *in vivo* models that showed the satisfactory biocompatibility and protective effects of PEG-RhZs on oxidative stress-induced degeneration of RPE cells as well as photoreceptors. In the early stage of AMD, the PEG-RhZs scavenged reactive oxygen species, alleviated RPE damage, and reduced the activation of inflammatory cells in the retina. In the late stage, PEG-RhZs exerted sustained protective effects, decreased the number of apoptotic photoreceptor cells, maintained normal retinal thickness and structure, and reduced vision loss. Our data demonstrate that PEG-RhZ can be a new strategy for the treatment of AMD (Scheme 1).

2. Methods

2.1. Synthesis and characterization of PEG-RhZs

The PEG-RhZs were synthesized by a reduction method [23,24]. The rhodium chloride hydrate (50 mg) and mPEG-SH (40 mg, 2000 Da) were dissolved in water (80 mL) and stirred under nitrogen flow for 30 min. Then, the sodium borohydride (2 mg/mL, 9 mL) was added dropwise to reduce rhodium chloride. After reaction for 5 min at room temperature, the dispersion was dialyzed in deionized water for 2 days (MWCO: 8–12 kDa), and the PEG-RhZs were collected by freeze-drying.

2.2. ROS-scavenging effects of PEG-RhZs

The antioxidant activities of PEG-RhZs were evaluated in the elimination efficacy toward different types of reactive oxygen and nitrogen species as our previous study [25].

2.3. Cell culture

ARPE-19 cells, BV2 cells and 661W cells were purchased from China Center for Type Culture Collection (CCTCC). BV2 cells were cultured in DMEM (GIBCO, Gaithersburg, MD, USA), while ARPE-19 cells and 661W cells in DMEM/F12 (GIBCO) supplemented with 10 % fetal bovine serum (GIBCO) and 1 % penicillin/streptomycin (Invitrogen) at 37 °C in a humidified atmosphere of 5 % CO_2.

2.4. Animals and experimental procedures

C57BL/6 mice (male, 8-week-old) were purchased from Gempharmatech (Nanjing, Jiangsu, China). Animals were given free access

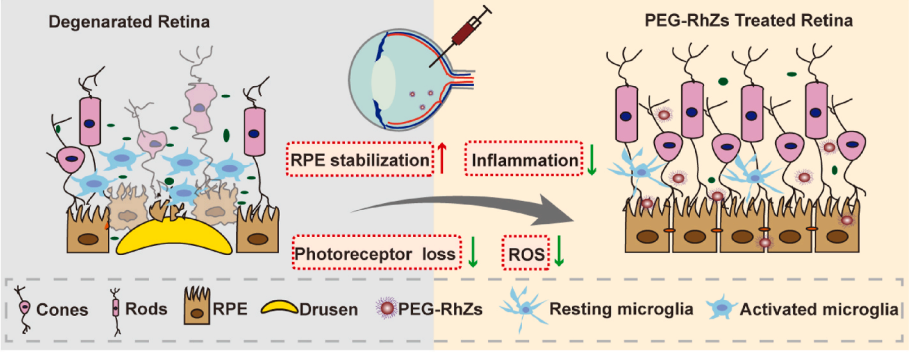

Scheme 1. Schematic illustration of therapeutic effects of PEG-RhZs for AMD. The PEG-RhZs scavenge ROS, inhibit microglia activation, alleviate RPE degeneration, stabilize the outer blood-retina barrier, and protect photoreceptors in AMD.

to food and water in a 12 h light/12 h dark cycle environment. All animal experiments were under the ARVO Statement for the Use of Animals in Ophthalmic and Vision Research and the guidelines approved by Animal Use and Care Committee of Tongji Hospital, at Huazhong University of Science and Technology, Wuhan, China.

Sterilized 0.5 % sodium iodate (SI) (Sigma-Aldrich, St. Louis, MO, USA) solution was freshly prepared, and diluted in phosphate-buffered saline (PBS). C57BL/6 mice were put in a plastic restrainer with a flexible stopper, and their tails were immersed in a 39–40 °C water bath for about a minute to cause sufficient dilatation of the lateral tail veins. Mice were injected with SI at a dosage of 35 mg/kg via the tail vein to induce RPE/retina degeneration. The control mice were injected with the same volumes of PBS.

PEG-RhZs were diluted in two concentrations: 500 ng/μL and 1000 ng/μL. Different doses of PEG-RhZs (1 μg/1 μL and 0.5 μg/1 μL) were intravitreally injected into the respective experimental eyes 1 day before SI injection. The sham group received intravitreal injection surgery with 1 μL PBS.

2.5. CCK-8 assay

CCK8 assay was conducted according to the manufacturer's protocol (Yeasen, #40203). Briefly, cells were seeded in 96-well plates and exposed to different treatments. After twice rinsed by PBS, each well was added with a mixture of 90 μL culture medium and 10 μL CCK8 solution, incubated at 37 °C for 1 h. The absorbance at 450 nm was measured by using a microplate reader (BioTek Instruments, USA).

2.6. Cell death analysis

Cells were incubated with a culture medium containing 5 μM Propidium iodide (Beyotime, #ST511) and 1 μM Hoechst (Beyotime, #C1011) for 30 min at 37 °C. After incubation, cells were washed with PBS for 3 times. Then observed and photographed by fluorescent microscope (Olympus, Tokyo, Japan) and PI-positive dead cells were counted by Fiji ImageJ software (Version 2.0.0).

2.7. RNA isolation and gene expression analysis

Total RNA was extracted using the RNAiso Plus (TaKaRa, #9109) and quantified with a spectrophotometer (NanoDrop, Thermo Fisher Scientific, USA). cDNA synthesis was performed with 500 ng of total RNA using PrimeScript RT Master Mix (Yeasen, #11123), in which the genomic DNA was removed by DNase I digestion. The gene expression level was analyzed by quantitative PCR (qPCR) with SYBR Green Supermix (Yeasen, #11201) using Applied Biosystems 7300 Real-Time PCR System (Thermo Fisher Scientific). Related primers are listed in Table S1.

2.8. RPE flatmount

After the mice were euthanized, the eyeballs were enucleated, and then the extraocular tissues were cut under a dissecting microscope. Tenotomy scissor was used to 360° circumferentially cut the eyeball at 3 mm posterior to the limbus. Two forceps were gently handled to separate the cornea, lens and retina from vessels from the RPE-eyecups. Four radial relaxing incisions were made on the isolated eyecups with the RPE facing up. The flatmount was then fixed in 4 % paraformaldehyde for 15 min and permeabilized with 0.1 % Triton X-100 for 30 min for further immunofluorescence procedures.

2.9. Immunofluorescence

Cells were seeded on glass coverslips and fixed in 4 % paraformaldehyde for 15 min at room temperature. After washed twice with PBS, cells were permeabilized with 0.1 % Triton X-100 for 15 min and blockd with 5 % BSA for 1 h at room temperature. After immunostained with primary antibodies at 4 °C overnight, incubated with the secondary antibody for 2h at room temperature and then counterstained for 15 min with Hoechst or DAPI.

For retina tissues, eyes were enucleated and immediately embedded by opti-mum cutting temperature compound (SAKURA, #4583) at −20 °C and then sectioned into 10 μm. Frozen sections and the RPE flat mounts for immunofluorescence were prepared using the same protocol as for the cells (see above). Images were captured with an inverted confocal microscope. Images were acquired using a confocal fluorescence microscope. The following antibodies were used for immunofluorescence: anti-ZO-1 (Invitrogen, #1A12), anti-Iba1 (CST, #117198), anti-NF-κB p65(CST, #8242), anti-IκBα (CST, #15595), FITC Phalloidin (YEASEN, #40735ES75), Alexa Fluor 488-labeled anti-rabbit IgG (CST, #4412), Alexa Fluor 594-labeled anti-rabbit IgG (CST, #8889), Alexa Fluor 488-labeled anti-mouse IgG (CST, #4408), Alexa Fluor 594-labeled anti-mouse IgG (CST, #8890).

2.10. Cellular ROS activity and in situ measurement of tissue ROS

ROS can hydrolyze nonfluorescent probe DCFH-DA to DCFH and subsequently convert it to fluorescent DCF [26]. Cellular ROS production was measured using a 2′,7′-dichlorofluorescein diacetate (DCFH-DA) assay kit (Beyotime, #S0033). Briefly, the cells in the six-well plates were rinsed and incubated with 25 mM DCFH-DA at 37 °C for 30 min. The fluorescence intensity was examined by inverted confocal microscope.

Dihydroethidium (DHE) was used to detect ROS levels in retinas as previously described [27]. Briefly, 10 μmol/L DHE (Beyotime, #S0063) was added to 10 μm unfixed fresh cryosections and incubated for 30 min at 37 °C. Images were captured using an inverted confocal microscope.

2.11. Paracellular permeability assay

The paracellular permeability of monolayer RPE cells was assessed by measuring the passive movements of fluorescein isothiocyanate (FITC)-dextran (70 kDa, Sigma-Aldrich) as previously described [28]. ARPE-19 cells were seeded in the upper chamber of Transwell filters (Costar, 12 mm diameter, 0.4 μm pore-size membrane) and allowed to grow until confluence (Fig. 3g). Subsequently, cells were treated with SI (10 mM) with or without PEG-RhZ (20 or 50 mg/mL) for 24 h at 37 °C. After treatment, the culture medium was changed and 1 mg/mL of FITC-dextran was added to the upper chamber. Samples (100 μL) were obtained from the upper and lower chambers 1.5 h after the addition of FITC-dextran. The fluorescence intensity of these samples was quantified by a microplate reader (Synergy2, BioTek, Winooski, VT, USA) at 485 nm of excitation and 528 nm of emission. The diffusion ratio (Diff) was calculated as follows: (Fluorescence intensity of FITC-dextran in the lower chamber)/(Fluorescence intensity of FITC-dextran in the upper chamber).

2.12. Scratch wound migration assay

BV2 cells were grown in 24-well plates till 70–80 % confluent. The monolayer of cells was then wounded with a sterile 10 μl pipette tip in a straight line along the diameter of the well. Images were captured at 0 h. Next, the original medium was replaced by a new medium according to different treatments. The cells were cultured for 24 h further, allowing migration into the open scratched area, and then images of cells were captured. The migration speed of BV2 cells was evaluated by counting the number of migrated cells in the wound place using the ImageJ software.

2.13. Protein extraction and western blot analysis

To extract total protein, cell lysis buffer (beyotime, #P0013J)

containing protease inhibitor cocktail (beyotime, #P1005) was added into harvested cells. In addition, cytoplasmic and nuclear proteins were extracted according to manuscript of the kit (beyotime, #P0027). Briefly, buffer A was added to harvested cells and following 5 s vortex, cytosol proteins in the supernatant were collected by centrifugation. Then nucleus in the precipitate were collected and nucleus protein were extracted by buffer B.

The protein samples were boiled for 10 min at 90 °C with loading buffer, separated with 10 % SDS-PAGE, and then transferred to polyvinylidene difluoride (PVDF) membranes. Subsequently, the membranes were blocked with 5 % nonfat milk in TBST for 1 h at room temperature. After that, the membranes were incubated overnight at 4 °C with primary antibodies. Then incubated with secondary antibodies for 1 h at room temperature. The protein was visualized by ECL kit (beyotime, #P0018) according to the manufacturer's instructions. Relative protein expression level was calculated by ImageJ software. Antibodies used for WB were listed as follows: anti- NF-κB p65(CST, #8242), anti-phospho-NF-κB p65(CST, #3033), anti-IκBα (CST, #15595), anti-phospho-IκBα (CST, #2859), anti-GAPDH (CST, #5174), Anti-rabbit IgG HRP-linked (CST, #7074), Anti-mouse IgG HRP-linked (CST, #7076).

2.14. Optomotor response (OMR) assay

The OMR assay was performed as previously described [29]. In brief, mice were placed in a dark environment for 2 h to acclimate before starting the test. The OMR instrument consisted of a central elevated platform and surrounding computer monitors. During the measurement process, mice could move freely on the elevated platform. Vertical sine wave gratings of different spatial frequencies were displayed on the surrounding screens and moved clockwise at a constant speed of 12°/s. The top camera recorded the mice's responses to different gratings. Gradually increased the spatial frequency of the grating until the animal no longer responded to it. This procedure was repeated 10 times for each mouse. The spatial frequency response threshold of each mouse was calculated through the software's program as visual acuity.

2.15. Histology and TUNEL staining

For histologic analysis, eyeballs from euthanized mice were fixed in FAS solution (Servicebio, #G1109) for 24h, and then gradient dehydration and embedding in paraffin. The embedded tissue was cut into 4 μm slices and stained by HE.

TUNEL staining was performed according to the manufacturer's protocol (meilunbio, #MA0224). The frozen sections of mice eyeballs were washed three times by PBS, 1 % Proteinase K was added for permeabilization, and then washed away by PBS. Freshly prepared TUNEL working solution was added and incubated with the tissue at 37 °C in the dark for 60 min in dark. The excess working solution was washed with PBS 3 times. TUNEL-positive cells in were outer nuclear layer (ONL) were observed by fluorescence microscope and outer nuclear layer of the retina and analyzed by image J.

2.16. 5-Ethynyl-2′-deoxyuridine (EdU) assay

The effects of PEG-RhZs on cell proliferation were measured by EdU assay kit (Abcam, #ab219801) following the instruction of manuscripts. In brief, the cells were incubated with 20 μM EdU labelling medium at 37 °C under 5 % CO_2 for 2 h and then fixed by 4 % paraformaldehyde. After incubation, the cells were washed twice and treated with permeabilization buffer for 20 min RT. Then EdU reaction cocktail was added to react with EdU for 30 min. Hoechst was used to stain cell nucleus after EdU reaction. Images of EdU positive cells were captured using an inverted fluorescence microscope. The number of EdU positive cells were calculated by imageJ.

2.17. ICP-MS

Ocular distribution of Rh after intravitreal injection PEG-RhZs were determined by ICP-MS. Animals were sacrificed at different timepoints (6 h, 12 h, 1 day and 30 days after 1 μg PEG-RhZs intravitreal injection) and their eyeballs were harvested. The contralateral eye injected with PBS was used as control. The eyeballs were incised along the corneoscleral limbus under anatomical microscope, and then the cornea, lens, retina and RPE-sclera tissues were carefully dissected by tweezers. The tissues were dissolved by HNO3 (1 % solution in DI water) and the dissolved tissue solution was filtered and injected into ICP-MS (Agilent 7800). The amount of Rh in each sample was represented by the mean of 3 repeated ICP-MS measurements.

2.18. Statistical analysis

All quantitative data were shown as mean ± standard deviation (SD). Statistical calculation was conducted with GraphPad Prism 7.0 software. Student t-test was used to compare the difference between two groups, while one-way ANOVA was used to analyze three groups and above. A p-value <0.05 was considered significant.

3. Results and discussion

3.1. Synthesis and enzymatic activities of PEG-RhZs

Rhodium nanoparticles with polyethylene glycol coatings (PEG-RhZs) were synthesized by the reduction of rhodium (III) chloride using SH-PEG as a polymeric stabilizer. Transmission electron microscopy (TEM) revealed that the PEG-RhZs had a spherical shape with an average diameter of 4.8 nm. High-resolution TEM (Fig. 1A and B) revealed the characteristic finger space of the Rh crystals. X-ray photoelectron spectroscopy (XPS) analysis (Fig. 1C) revealed the characteristic peaks of Rh 3d, assigned to Rh (0) (306.2 eV, 310.9 eV) and Rh (III) (307.8 eV, 312.5 eV). The enzymatic activities of PEG-RhZs toward scavenging different types of reactive species were investigated (Fig. 1D–F). We first determined the superoxide dismutase (SOD)-like activity of PEG-RhZs on eliminating $O_2^{\bullet-}$ using the nitro blue tetrazolium (NBT) photochemical reduction method [24]. PEG-RhZs effectively eliminated $O_2^{\bullet-}$ in a dose-dependent manner, and the clearance rate reached 90.1 % at a concentration of 100 μg/mL. Similarly, PEG-RhZs significantly scavenged H_2O_2 in a dose-dependent manner, suggesting good catalase (CAT)-like activity. In addition, PEG-RhZs could also remove reactive nitrogen species (RNS), which was examined using 2, 2-di-(4-tert-octylphenyl)-1-picrylhydrazyl (DPPH). Over 80 % of $DPPH^{\bullet}$ (200 μg/mL) was eliminated by PEG-RhZs (50 μg/mL). These results suggest that PEG-RhZs could effectively eliminate both ROS and RNS and could be potent antioxidant agents.

3.2. Biocompatibility of PEG-RhZs in vitro and in vivo

The viability of retinal cells and immune cells that could be readily exposed to PEG-RhZs was analyzed by a CCK8 assay. ARPE-19 cells (retinal pigment epithelial cell line), 661 W cells (photoreceptor cell line), and BV2 cells (microglial cell line) were subjected to PEG-RhZs at various doses (from 10 to 100 μg/mL) for 24 h. PEG-RhZs did not affect cell viability at a concentration of 100 μg/mL in any of these cells, as the cell viability was still greater than 95 % after 24 h of exposure (Fig. 2A–C). In addition, to assess the impact of PEG-RhZs on cell proliferation, 5-Ethynyl-2′-deoxyuridine (EdU) assay was conducted to directly detect DNA synthesis in cells through EdU incorporation and subsequent click reaction [30]. Consistent with the CCK8 results, there was no significant difference in EdU staining rate between PEG-RhZs treated group and control group (Figs. S3A–D).

In vivo biosafety was evaluated after intravitreal injection of PEG-RhZs (1 μg per mouse) for 1 month. TUNEL assays revealed that PEG-

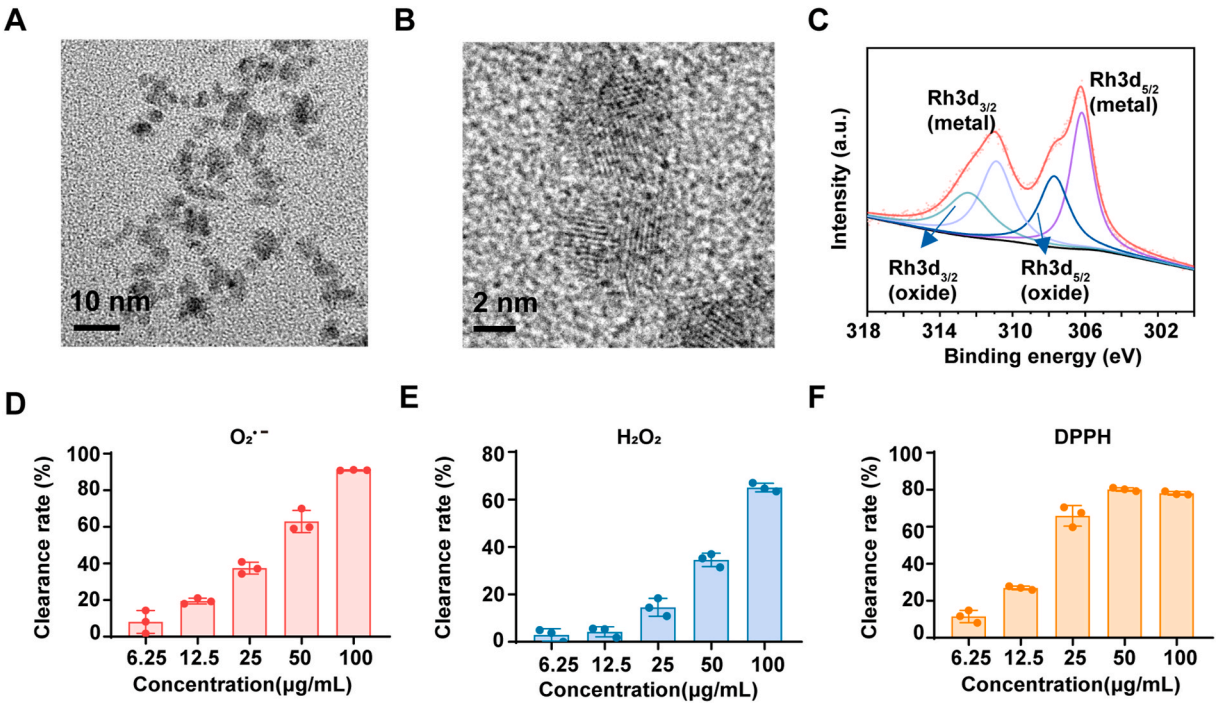

Fig. 1. Characterization of PEG-RhZs. (A) TEM image of PEG-RhZs. Scale bar, 10 nm. (B) TEM image of PEG-RhZs. Scale bar, 2 nm. (C) XPS spectra of PEG-RhZs. $O_2^{\bullet-}$ (D), H_2O_2 (E), and DPPH (F) scavenging abilities of PEG-RhZs at different concentrations.

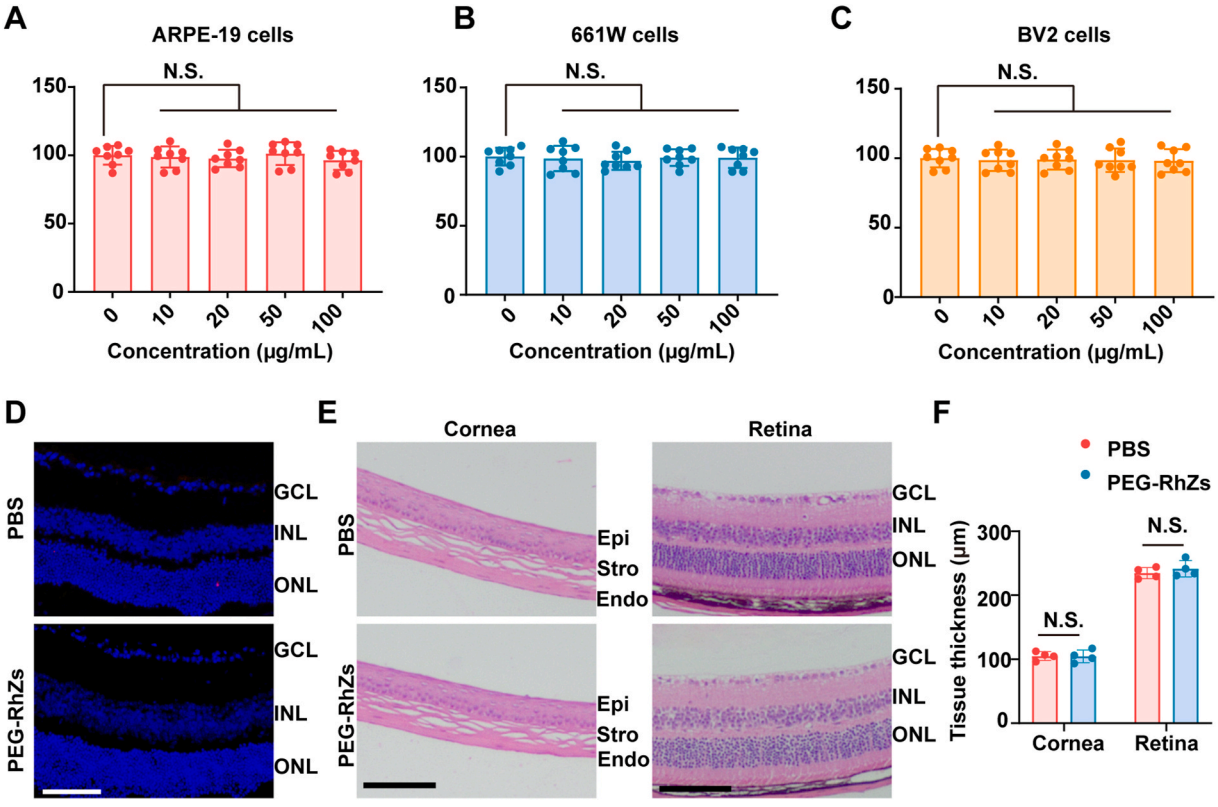

Fig. 2. Biocompatibility of PEG-RhZs. (A–C) Cell viability of ARPE-19 cells (A), 661W cells (B), and BV2 cells (C) treated with PEG-RhZs (0, 10, 20, 50, 100 μg/mL) for 24 h n = 8. Data were presented as the mean ± SD. (D) 1 month after PEG-RhZs (1 μg) were intravitreously injected, and the number of apoptotic cells in retinas was evaluated by TUNEL. Scale bar, 50 μm. n = 4. (E, F) Representative HE staining images of cornea and retina and quantitative analysis of their thickness. Scale bar, 100 μm. n = 4. Data were shown as mean ± SD. N.S., not significant.

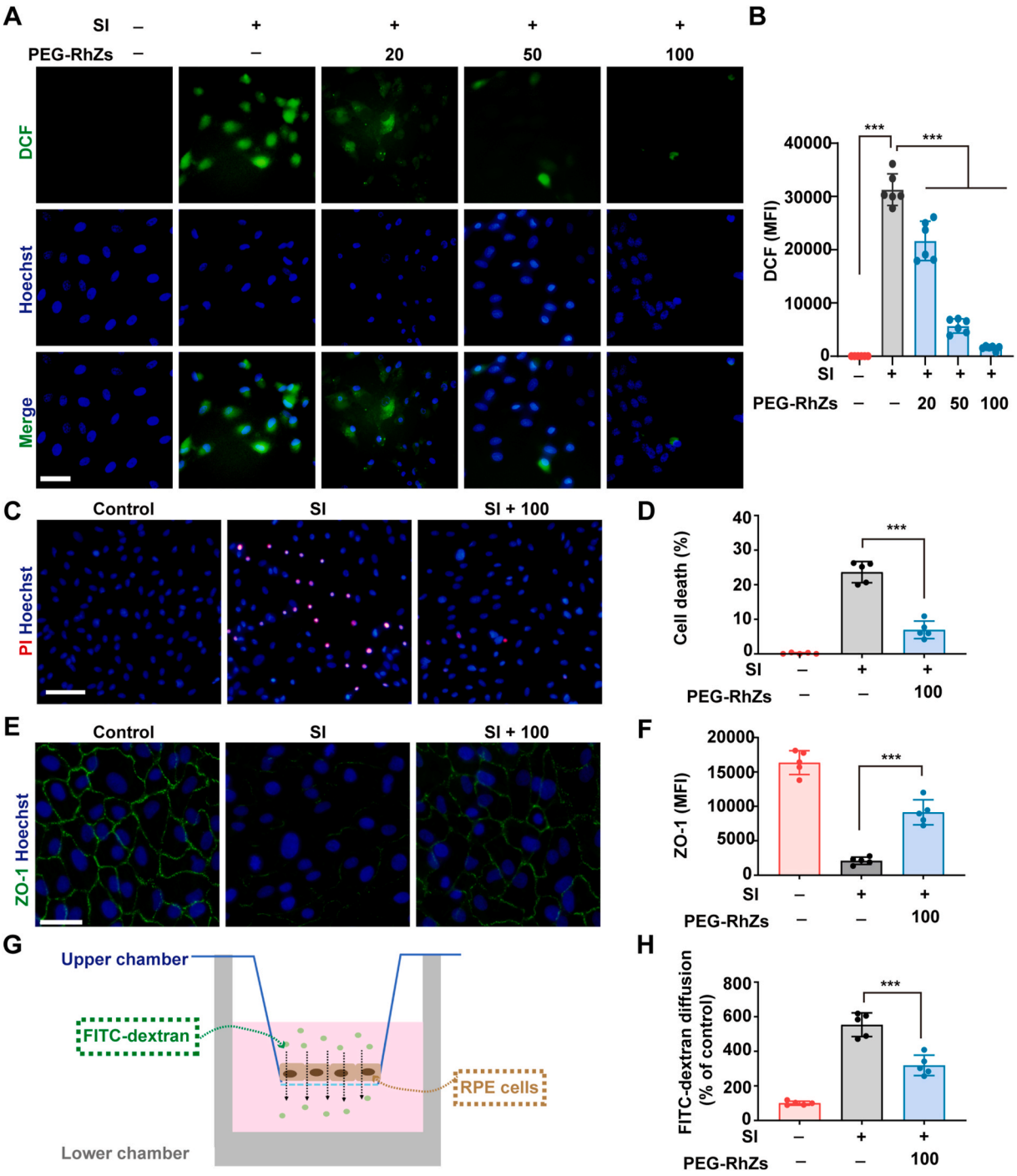

Fig. 3. PEG-RhZs scavenged ROS and protected RPE cells. ARPE-19 cells were treated with SI (2 mM) and PEG-RhZs (20, 50, and 100 μg/mL) for 24 h. (A, B) Representative fluorescence images of ROS by DCFH-DA assay and statistic analysis of the mean fluorescence intensity (MFI). Scale bar, 30 μm. n = 6. (C, D) Representative images and quantitative analysis of cell death by PI staining. Scale bar, 80 μm. n = 5. (E, F) Representative ZO-1 staining of ARPE-19 cells and quantitation of MFI. Scale bar, 30 μm. n = 5. (G) Schematic of paracellular permeability assay. (H) Quantitation of FITC-dextran diffusion through the RPE monolayer. n = 5. Data were presented as mean ± SD. *P < 0.05, **P < 0.01, ***P < 0.001.

RhZ injection did not lead to retinal cell death (Fig. 2D and Fig. S2). Additionally, HE staining revealed that PEG-RhZs did not change the structure or morphology of eye tissues, such as the anterior segment cornea and posterior segment retina (Fig. 2E and F), further demonstrating that PEG-RhZs are not toxic to the eyes. Subsequently, fresh red blood cells isolated from the whole blood of C57BL/6 mice were utilized to assess the potential risk of hemolysis. No discernible hemolysis was observed after incubation with PEG-RhZs varying from 0 to 100 μg/mL at 37 °C for 4 h (Fig. S4A). Quantitative analysis revealed that even at relatively high concentrations (100 μg/mL) of PEG-RhZs, the degree of hemolysis remained below 1 % (Fig. S4A). Moreover, fresh whole blood were harvested before and at 1 day and 30 days post intravitreal injection of 1 μg PEG-RhZs. There were no significant alterations in typical hematological parameters (Figs. S4B–E) such as red blood cells (RBCs), white blood cells (WBCs), platelets (PLTs), and hemoglobin (HGB). Our results were consistent with previous reports at other tissue and cell levels [20–22], confirming the good biocompatibility of PEG-RhZs.

3.3. PEG-RhZs protected RPE cells from ROS stimulation

ROS accumulation-induced RPE degeneration is the key pathogenesis of AMD [1,3,4]. The RPE cells situated between the photoreceptor and the choroid, is a highly metabolically active cell responsible for continuous phagocytosis of shed outer segment membrane disks from the photoreceptor, absorption of light scattering, and provision of nutrients to the photoreceptor [31]. Prolonged exposure to light leads to accumulation of reactive oxygen species and photo-oxidized lipids and proteins, exacerbating oxidative damage in RPE [31]. Considering the ROS scavenging capability of PEG-RhZs, we detected the ROS levels in the SI-treated ARPE-19 cells treated with and without PEG-RhZs by DCFH-DA. Consistent with previous reports [32,33], ROS levels in ARPE-19 cells were significantly increased after 24 h of SI (2 mM) stimulation (Fig. 3A and B). However, intracellular ROS levels were obviously decreased upon PEG-RhZ treatment in a dose-dependent manner. Moreover, SI-induced oxidative damage was abrogated by PEG-RhZs. RPE cell viability increased from 46.96 % to 86.06 % as the concentration of PEG-RhZs increased from 0 to 100 μg/mL (Fig. S1). The anti-ROS and cell protection effects of PEG-RhZs were further confirmed by PI staining. The SI-induced RPE cell death rate decreased more than 3-fold when 100 μg/mL PEG-RhZs was added (Fig. 3C and D).

RPE plays a crucial role in maintaining the integrity of the outer blood-retinal barrier, regulating the transport of essential nutrients and toxic molecules between the retina and choroid [31]. ROS accumulation disturbs ZO-1 expression and leads to RPE barrier function loss [34]. In our *in vitro* ROS-induced RPE model, ZO-1 almost completely disappeared (Fig. 3E and F), and the permeability of the RPE monolayers to

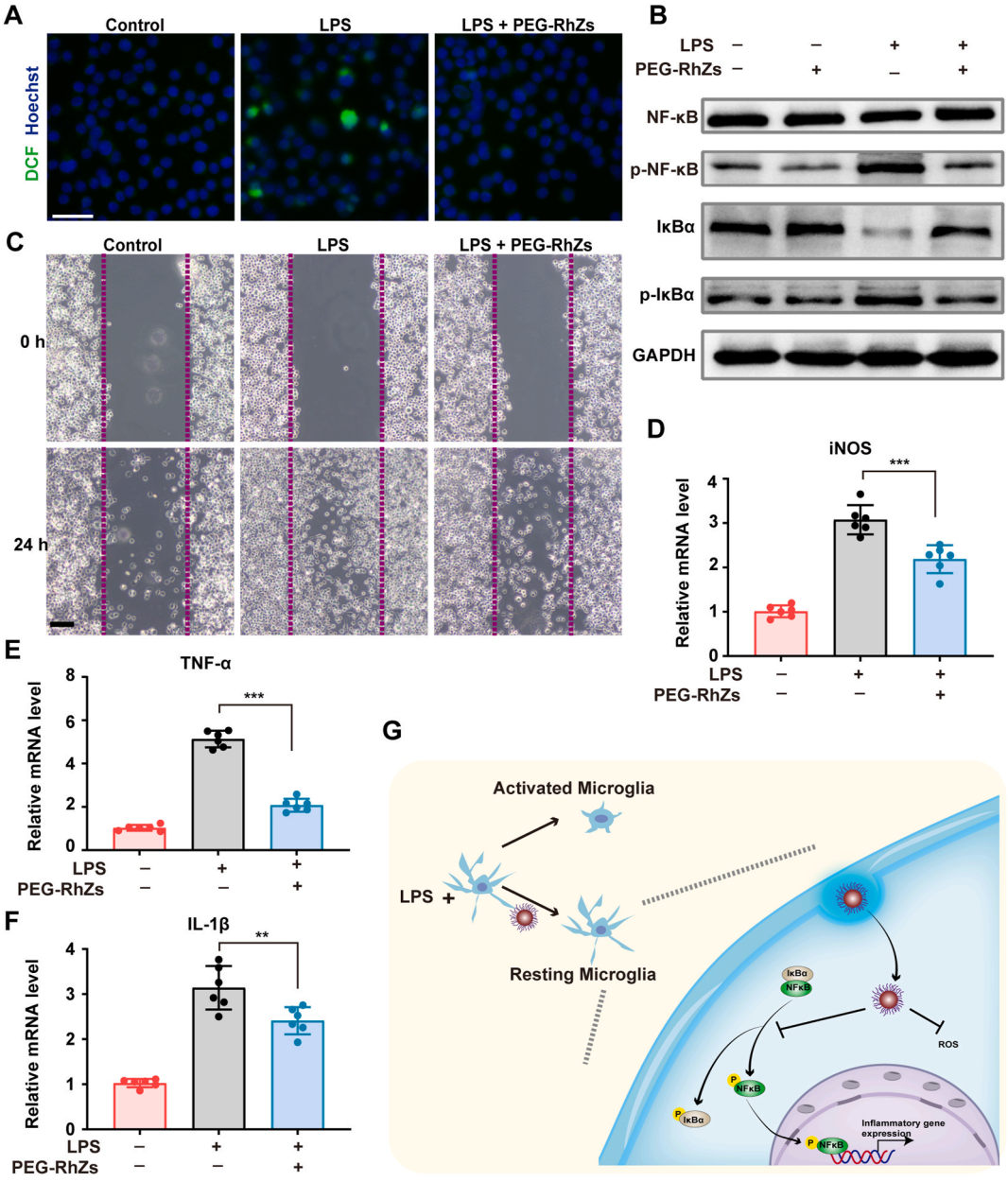

Fig. 4. PEG-RhZs inhibited microglia inflammatory response. (A) Intracellular ROS levels of BV2 cells by DCFH-DA. Scale bar, 30 μm. n = 5. (B) Western Blot analysis of total NF-κB p65, Phospho-NF-κB p65, total IκBα, Phospho-IκBα and GAPDH protein expression in BV2 cells upon different treatments. n = 5. (C) Wound healing assay analysis of migrated BV2 cells. Scale bar, 100 μm. n = 6. (D–F) Relative mRNA expression of iNOS, TNF-α and IL-1β in BV2 cells examined by quantitative PCR (qPCR). n = 6. Data were presented as the mean ± SD. **P < 0.01, ***P < 0.001. (G) Schematic of the anti-inflammatory process of PEG-RhZs on microglia.

FITC-dextran increased more than 5-fold (Fig. 3G and H). Notably, PEG-RhZs remarkably maintained ZO-1 expression and the barrier function of the RPE upon SI stimulation (Fig. 3E–H). The protective effects of PEG-RhZs on ZO-1 expression and barrier function of the RPE cells hinted its potency of maintaining blood-retinal barrier integrity and retinal homeostasis.

3.4. PEG-RhZs inhibited the microglial inflammatory response

In addition to RPE degeneration, ROS leads to overreactive neurotoxic microglia, which release numerous proinflammatory and cytotoxic factors, including tumor necrosis factor-α (TNF-α), further aggravating AMD progression [4,6]. Thus, we next observed the effects of PEG-RhZs on microglial activation. It has been widely reported that lipopolysaccharide (LPS) stimulation can activate microglia and promote proinflammatory mediator expression [35,36]. LPS (1 μg/mL) was used to activate the murine BV2 microglial cell line. Similar to their role in RPE cells, PEG-RhZs significantly cleared LPS-induced ROS (Fig. 4A and Fig. S5A). In addition, the qPCR results showed that the increase in the levels of inducible NO synthase (iNOS), TNF-α and IL-1β induced by LPS was inhibited by PEG-RhZs (Fig. 4D–F). Under pathological conditions, iNOS might continuously produce high levels of NO to exacerbate neuronal damage and upregulate inflammatory mediators to recruit more inflammatory cells [37,38]. The downregulation of iNOS by PEG-RhZs disrupts a critical step in the vicious cycle of inflammation and tissue damage.

The inflammatory processes, exacerbated by TNF-α and IL-1β, were considered as pivotal events in the pathogenesis of AMD. IL-1β exhibits potent pro-inflammatory activity and can stimulate the production of various pro-inflammatory mediators, including cytokines and chemokines [39]. Locally, IL-1 signaling leads to upregulation of adhesion molecules, facilitating lymphocyte recruitment and further amplification of inflammation [39]. In oxidative stress damaged retinas, activated neurotoxic microglia release IL-1β, thereby creating a pro-inflammatory environment that promotes recruitment of retinal microglia and infiltration of monocytes from external sources, ultimately resulting in progressive degeneration of photoreceptors [17,18]. Besides, IL-1β can induce secretion of VEGF, and treatment with IL-1Ra, an inhibitor of IL-1β, can significantly suppress CNV. The excellent IL-1β inhibition effects of PEG-RhZs on LPS stimulated BV2 cells suggested its therapeutic potential in immune disorder related disease, such as AMD, inflammatory bowel disease, and arthritis. TNF-α is also a pleiotropic pro-inflammatory cytokine implicated in various diseases. It can up-regulates VEGF production by activating β-catenin, thereby promoting the formation of choroidal neovascularization (CNV). Conversely, treatment with anti-TNF-α reduces the size and leakage of CNV in mice. In addition, increased expression of TNF-α has been observed in patients with dry AMD. Therefore downregulation of TNF-α through PEG-RhZs treatment might alleviate the progression of AMD, including CNV formation and leakage.

The increased migration of microglia in response to inflammatory factors is an indicator of neuroinflammation [40]. Hence, we determined the effects of PEG-RhZs on BV2 cell migration. As shown in the scratch wound migration assay, the increase in cell migration induced by LPS treatment was significantly reversed by PEG-RhZs (Fig. 4C and Fig. S5B). To further investigate the inhibitory mechanism of PEG-RhZs on the BV2 inflammatory response, the NF-κB signaling pathway, which regulates the expression of many inflammatory genes [41], was detected by western blot. We found that PEG-RhZs alone did not influence the protein levels of total NF-κB p65, phospho-NF-κB p65 (p-NF-κB p65), total IκBα or phospho-IκBα (p-IκBα). While, in LPS-activated BV2 cells, PEG-RhZs treatment inhibited the phosphorylation of NF-κB p65 and IκBα and upregulated total IκBα (Fig. 4B and Figs. S5C–D). There was no significant change of total NF-κB p65 protein level among PEG-RhZs, LPS and LPS + PEG-RhZs groups (Fig. 4B). Upon LPS stimulation, the IKK complex phosphorylated IκBα which then was ubiquitinated and degraded, while NF-κB p65 translocated to the nucleus and regulated gene transcription [42]. Due to the significant inhibition effects of PEG-RhZs on phosphorylation of NF-κB p65 and IκBα, we further detected the nuclear localization of NF-κB p65. Nucleocytoplasmic separation assay and immunofluorescence (Figure S5E-H and Figure S6A-B) showed nuclear translation of NF-κB p65 was significantly suppressed by PEG-RhZs through upregulation of cytoplasmic IκBα. Taken together, the phosphorylation of IκBα and NF-κB p65 triggered the nuclear translocation of NF-κB p65 and transcriptionally activated downstream inflammatory gene expression (Fig. 4H). In conclude, these results suggested that PEG-RhZs effectively suppressed LPS-induced ROS production, NF-κB activation, proinflammatory factor expression, and BV2 cell migration, which might be used to alleviate neuroinflammation in AMD.

3.5. Therapeutic effects of PEG-RhZs during the acute period in the AMD model

To avoid nasolacrimal drainage and the barrier of cornea, anterior chamber and lens, PEG-RhZs were administered by intravitreal injection. The in ocular biodistribution of PEG-RhZs was determined by ICP-MS at 6 h, 12 h, 1 day, 7 days and 30 days after intravitreal injection of 1 μg PEG-RhZs. Rh contents in cornea, lens, and retina peaked 12 h after injection while the Rh content in RPE-Sclera peaked 1 day after injection. The peak values of Rh in cornea, lens, retina and RPE-Sclera were 0.0082 μg/g, 0.0466 μg/g, 1.8955 μg/g and 1.4994 μg/g respectively (Figs. S7A–D). These results demonstrated that intravitreal injection of PEG-RhZs were suitable to treat retinal and RPE related disease. Furthermore, Rh in cornea and lens were cleared 30 days postinjection as there were no difference between PEG-RhZs group and PBS group, while small amount of Rh still existed in the retina and RPE-Sclera (Fig. S7E). Prolonged retention of PEG-RhZs allowed for avoidance of repeated injection.

SI administration specifically induces RPE oxidative damage, and subsequent retinal neurodegeneration has been well documented as AMD model [32,33,43–45]. We generated an SI-induced AMD model and investigated the potential therapeutic efficacy of PEG-RhZs. Schematic illustrations of the administration approach and timeline are provided in Fig. 5A. The ROS content in the retina was assessed by superoxide-sensitive fluorescent dye dihydroethidium (DHE). DHE staining revealed that the SI-induced increase in ROS levels was reduced by PEG-RhZs in a dose-dependent manner (Fig. 5B and Fig. S8). Quantitative analysis revealed that ROS in the retina decreased 5-fold after a single intravitreal injection of 1 μg of PEG-RhZs (Fig. S8), suggesting that PEG-RhZs markedly attenuated SI-induced oxidative stress in the retina. The morphology and barrier function of the mouse RPE were determined by phalloidin staining for F-actin and ZO1 staining for tight junction proteins respectively. The results indicated that SI treatment disrupted the hexagonal structure of the RPE and the interconnections between cells, while PEG-RhZs restored the cytoskeletal structure and ZO1 expression in the RPE (Fig. 5C and D). The results of the *in vivo* experiments were consistent with those of the *in vitro* experiments in ARPE-19 cells (Fig. 3E–H), which confirmed the protective effects of the PEG-RhZs on the structure and function of the RPE under ROS stimulation.

Because of the excellent anti-inflammatory effects of PEG-RhZs on microglia *in vitro*, we sought to verify whether PEG-RhZs could be applied to retinal inflammation *in vivo*. Immunofluorescence staining for the microglial marker Iba1 revealed that the number of microglia with an activated amoeboid-like morphology significantly increased 7 days after SI administration, while PEG-RhZs greatly alleviated microglial activation and infiltration in the mouse retina (Fig. 5E and Fig. S9). As microglia are the major form of innate immune cells in the retina and participate in retinal neuroinflammation [6,7], the inhibition of microglia by PEG-RhZs could suppress the retinal inflammatory microenvironment in AMD.

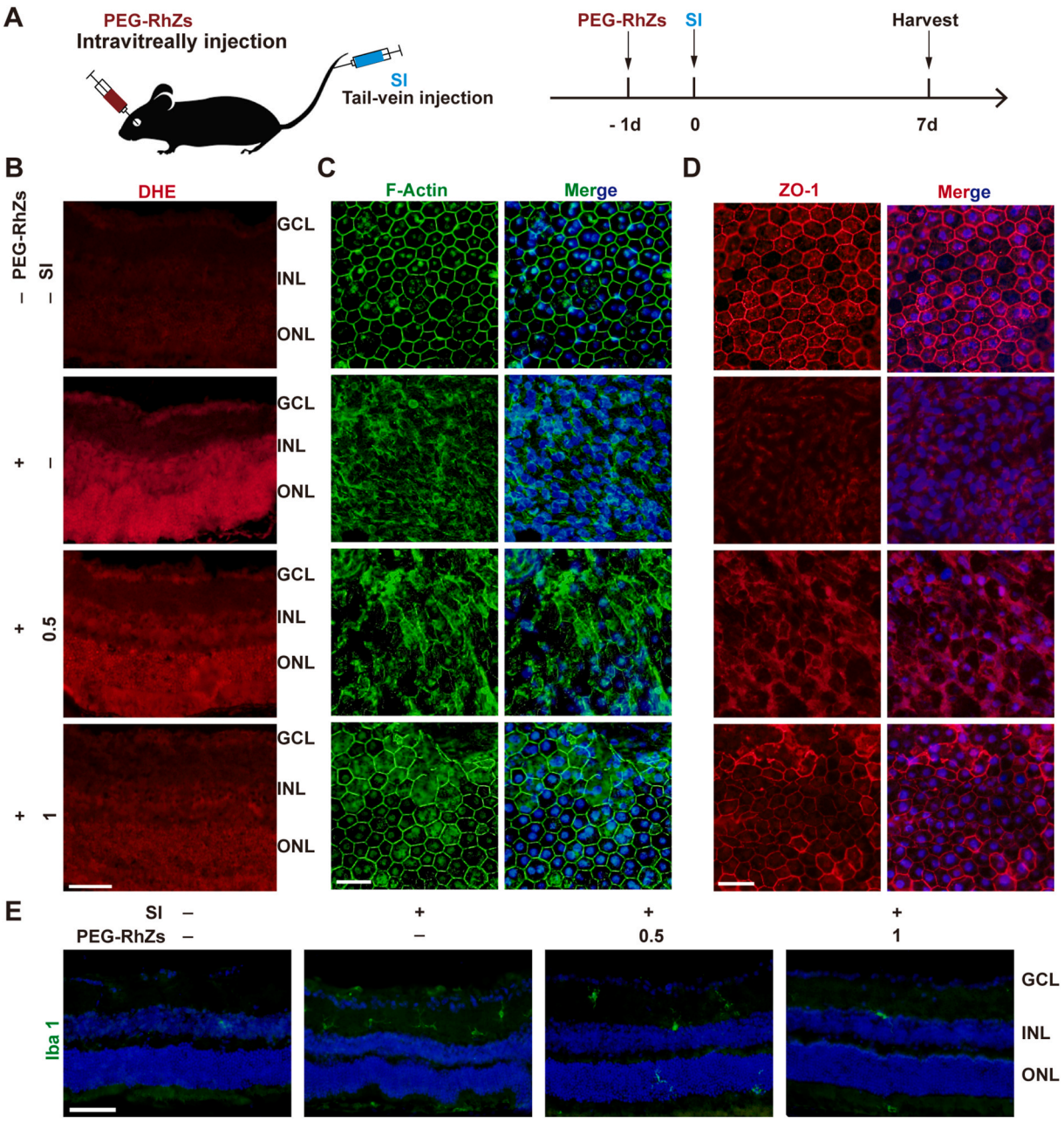

Fig. 5. PEG-RhZs alleviated SI-induced retinal oxidative stress, microglia activation, and RPE damage. (A) The administrative procedure and timeline are schematized. (B) In situ superoxide in the retina is indicated by dihydroethidium (DHE) staining. Scale bar, 50 μm. n = 5. (C, D) F-action and ZO-1 staining of RPE flatmount. Scale bar, 50 μm. n = 5. (E) Iba1 staining of retina sections. Scale bar, 50 μm. n = 5.

3.6. Therapeutic effects of PEG-RhZs in the late stage of AMD

One advantage of the application of nanozymes in biomedicine is that their pharmacokinetics, such as biodistributions, clearances, and long-term fates, can be determined by regulating their size, composition, surface charge, surface coating, or state of agglomeration [46]. In drug-induced liver injury (DILI), ceria nanozymes (CeNZs) exhibited a prolonged therapeutic window compared to that of N-acetylcysteine (NAC) and benefited patients in the late DILI stage [47]. Following with RPE degeneration and inflammatory cell activation, ROS and inflammation lead to photoreceptor death and vision loss with disease progression [10,48,49]. Thus, to investigate the long-term effects of PEG-RhZs on the SI-induced AMD model, we checked the retina and vision function of the mice at 1month post intravitreal injection (Fig. 6A).

The use of a virtual optomotor task to measure spatial visual thresholds is a commonly used vision function test method [49,50]. The OMR results showed that PEG-RhZ treatment elevated the spatial threshold frequency of the mice, especially in the 1 μg PEG-RhZ-treated group, indicating that PEG-RhZ effectively protected the vision of the mice in the AMD model (Fig. 6B and C). TUNEL staining of the retina partially explained the vision-protective effects of PEG-RhZs (Fig. 5D and Fig. S10), as photoreceptor cell death was obviously attenuated by PEG-RhZs. Moreover, histologic examinations indicated that the accumulation of pathological debris almost disappeared and the structure of photoreceptors restored after PEG-RhZ administration (Fig. 6E). The thickness of the retina outer nuclear layer (ONL), which represents the nucleus of the photoreceptors, was measured in the central and peripheral retina and quantified separately (Fig. S11). The quantitative analysis of ONL thickness showed that PEG-RhZs mitigated

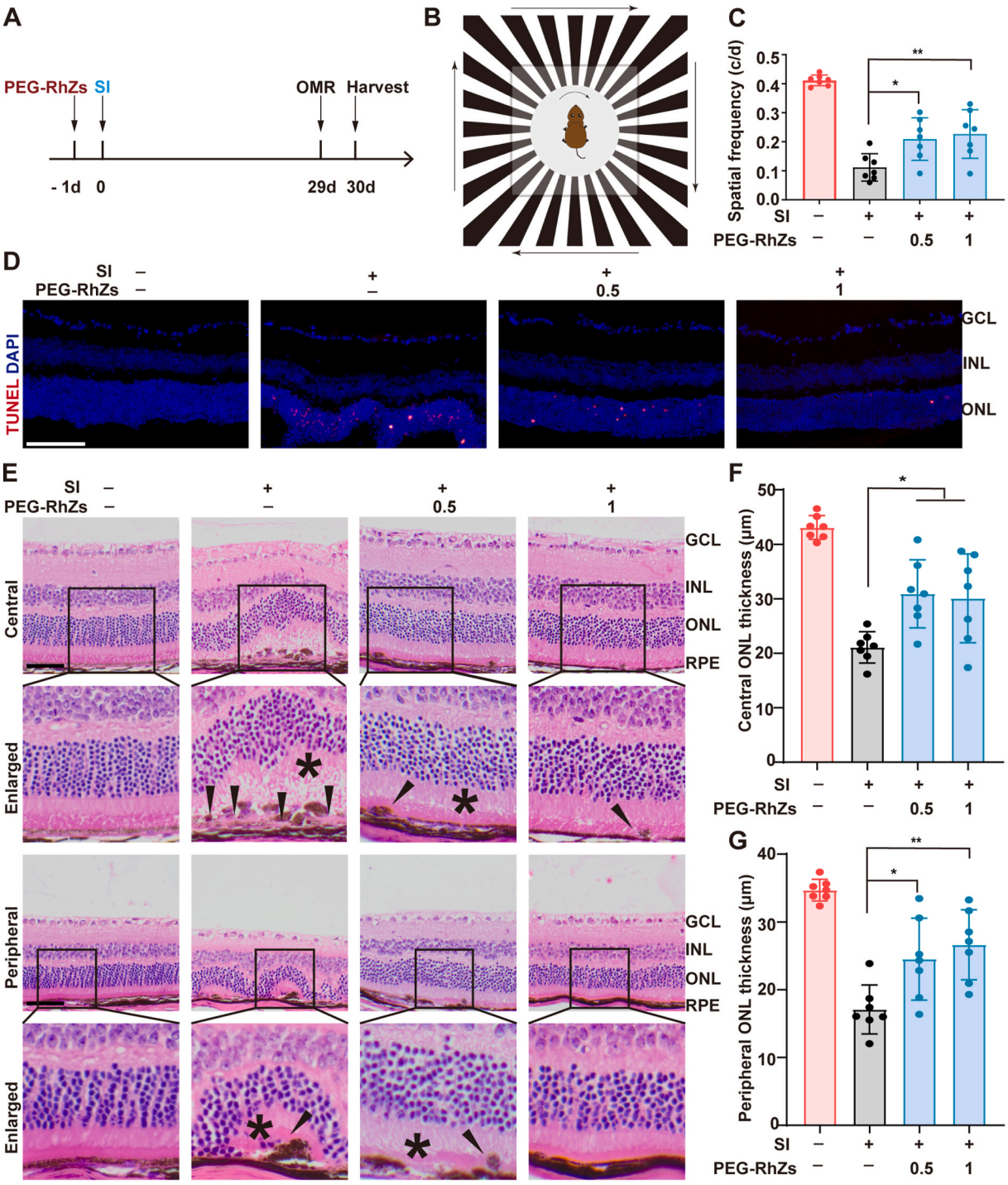

Fig. 6. PEG-RhZs protected photoreceptors and mice vision at a late stage. (A) The timeline of administrative procedure. (B) The schematic of OMR assay. (C) Quantitative analysis of threshold spatial frequency in OMR test. n = 7. (D) TUNEL staining of retina sections. Scale bar, 50 μm. n = 7. (E) HE staining of retina sections. The retinal photoreceptor external segments (POS) were disrupted (black stars) and drusen-like deposition formed (black arrows). Scale bar, 50 μm. n = 7. (F, G) The ONL thickness of the central and peripheral retina was quantified. n = 7. Data were presented as mean ± SD. *P < 0.05, **P < 0.01, ***P < 0.001.

photoreceptor loss in both the central and peripheral retina (Fig. 6F and G). These results suggested that PEG-RhZs had long-term protective effects on photoreceptor cells and vision function in the AMD model.

4. Conclusion

AMD is attributed to various complex causes, such as retinal pigment epithelial damage from oxidative stress, inflammatory activation, and photoreceptor damage [4,6]. Previous studies have shown that some small molecule antioxidants and natural antioxidants possess certain antioxidant effects, but their limited use is due to issues like poor pharmacokinetics, inadequate activity and stability, and safety problems [32,45]. To address these challenges, nanomaterials with superior properties were explored to prevent AMD.

PEG-RhZs Nanozymes with ROS and RNS activities were developed. The PEG-RhZs can efficiently eliminate overproduced intracellular oxidatively active substances and exhibit good biocompatibility with retinal cells, immune cells and ocular tissues such as the cornea and

retina. Apart from its antioxidant properties, PEG-RhZ also hinders microglial activation and the release of pro-inflammatory factors by suppressing NF-κB activation. A single intravitreal injection of PEG-RhZs can safeguard RPE cells from oxidative stress and impede microglia activation in the retina. Even after thirty days post-injection, PEG-RhZ continues to offer protection to photoreceptor cells and can mitigate vision loss in AMD model mice.

In summary, we developed an Rh-based nanozyme that mimics the natural antioxidant enzyme abilities. Upon a single intravitreal injection, it efficiently eliminates reactive oxygen species and exhibits prolonged efficacy in retinal degeneration. This study sheds light on the advancement of nanozymes with versatile enzyme-mimicking capabilities and presents promising alternatives for AMD treatment.

CRediT authorship contribution statement

Qian Sun: Writing – original draft, Investigation, Formal analysis. **Yueqi Ni:** Formal analysis. **Kang Wang:** Formal analysis. **Hong Zhang:** Supervision, Funding acquisition. **Jia Liu:** Writing – review & editing, Supervision, Funding acquisition, Conceptualization. **Lingjuan Xu:** Writing – review & editing, Supervision. **Yin Zhao:** Writing – review & editing, Supervision, Funding acquisition, Conceptualization.

Declaration of competing interest

The authors declare that they have no known competing financial interests or personal relationships that could have appeared to influence this research article.

Data availability

Data will be made available on request.

Acknowledgements

This work was supported by the Tongji Hospital scientific research project 2023A19 to Yin Zhao, National Natural Science Foundation of China Grant no. 82271090 to Hong Zhang and no. 82072068 to Jia Liu. Natural Science Foundation of Hubei Province of China Grant no. 2024AFA053 to Jia Liu, and Tongji Hospital scientific research project 2023A19 to Yin Zhao. The authors thank the Experimental Medicine Center of Tongji Hospital (Tongji Medical College, Huazhong University of Science and Technology) for providing support for the experiments.

Appendix A. Supplementary data

Supplementary data to this article can be found online at https://doi.org/10.1016/j.mtbio.2024.101230.

References

[1] P. Mitchell, et al., Age-related macular degeneration, Lancet 392 (10153) (2018) 1147–1159.
[2] J.M. Colijn, et al., Prevalence of age-related macular degeneration in europe: the past and the future, Ophthalmology 124 (12) (2017) 1753–1763.
[3] S. Datta, et al., The impact of oxidative stress and inflammation on RPE degeneration in non-neovascular AMD, Prog. Retin. Eye Res. 60 (2017) 201–218.
[4] Y. Deng, et al., Age-related macular degeneration: epidemiology, genetics, pathophysiology, diagnosis, and targeted therapy, Genes Dis 9 (1) (2022) 62–79.
[5] S. Nashine, Potential therapeutic candidates for age-related macular degeneration (AMD), Cells 10 (9) (2021).
[6] W. Tan, et al., The role of inflammation in age-related macular degeneration, Int. J. Biol. Sci. 16 (15) (2020) 2989–3001.
[7] M. Boyce, et al., Microglia-neutrophil interactions drive dry AMD-like pathology in a mouse model, Cells 11 (22) (2022).
[8] F. Cruz-Guilloty, et al., Infiltration of proinflammatory m1 macrophages into the outer retina precedes damage in a mouse model of age-related macular degeneration, Int J Inflam 2013 (2013) 503725.
[9] C.M. Eandi, et al., Subretinal mononuclear phagocytes induce cone segment loss via IL-1beta, Elife 5 (2016).
[10] K. Kiuchi, et al., Morphologic characteristics of retinal degeneration induced by sodium iodate in mice, Curr. Eye Res. 25 (6) (2002) 373–379.
[11] S. Schnichels, et al., Retina in a dish: cell cultures, retinal explants and animal models for common diseases of the retina, Prog. Retin. Eye Res. 81 (2021) 100880.
[12] M.V. Cicinelli, et al., Optical coherence tomography angiography in dry age-related macular degeneration, Surv. Ophthalmol. 63 (2) (2018) 236–244.
[13] M.J. Tolentino, A.J. Tolentino, Investigational drugs in clinical trials for macular degeneration, Expert Opin Investig Drugs 31 (10) (2022) 1067–1085.
[14] Y. Huang, J. Ren, X. Qu, Nanozymes: classification, catalytic mechanisms, activity regulation, and applications, Chem Rev 119 (6) (2019) 4357–4412.
[15] J. Yang, et al., Bioinspired copper single-atom nanozyme as a superoxide dismutase-like antioxidant for sepsis treatment, Exploration (Beijing) 2 (4) (2022) 20210267.
[16] J. Wu, et al., Nanomaterials with enzyme-like characteristics (nanozymes): next-generation artificial enzymes (II), Chem. Soc. Rev. 48 (4) (2019) 1004–1076.
[17] J. Chen, et al., Rare earth nanoparticles prevent retinal degeneration induced by intracellular peroxides, Nat. Nanotechnol. 1 (2) (2006) 142–150.
[18] L. Fiorani, et al., Cerium oxide nanoparticles reduce microglial activation and neurodegenerative events in light damaged retina, PLoS One 10 (10) (2015) e0140387.
[19] M. Alrobaian, Pegylated nanoceria: a versatile nanomaterial for noninvasive treatment of retinal diseases, Saudi Pharm J 31 (10) (2023) 101761.
[20] G.J. Cao, et al., Intrinsic catalytic activity of rhodium nanoparticles with respect to reactive oxygen species scavenging: implication for diminishing cytotoxicity, J. Environ. Sci. Health C Environ. Carcinog. Ecotoxicol. Rev. 37 (1) (2019) 14–25.
[21] Z. Miao, et al., Ultrasmall rhodium nanozyme with RONS scavenging and photothermal activities for anti-inflammation and antitumor theranostics of colon diseases, Nano Lett. 20 (5) (2020) 3079–3089.
[22] H.J. Zhong, et al., A rhodium(III) complex as an inhibitor of neural precursor cell expressed, developmentally down-regulated 8-activating enzyme with in vivo activity against inflammatory bowel disease, J. Med. Chem. 60 (1) (2017) 497–503.
[23] Z. Miao, et al., Ultrasmall rhodium nanozyme with RONS scavenging and photothermal activities for anti-inflammation and antitumor theranostics of colon diseases, Nano Lett. 20 (5) (2020) 3079–3089.
[24] J. Liu, et al., Ultrasmall ruthenium nanozyme with RONS scavenging and anti-inflammatory effects for effective prevention of postoperative peritoneal adhesion, Chem. Eng. J. 485 (2024) 150001.
[25] J. Liu, W.Y.S. L, Ruthenium-based metal-organic framework with reactive oxygen and nitrogen species scavenging activities for alleviating inflammation diseases, Nano Today (47) (2022) 101627.
[26] H. Bai, et al., Prussian blue nanozymes prevent anthracycline-induced liver injury by attenuating oxidative stress and regulating inflammation, ACS Appl. Mater. Interfaces 13 (36) (2021) 42382–42395.
[27] H. Song, et al., NADPH oxidase contributes to photoreceptor degeneration in constitutively active RAC1 mice, Invest. Ophthalmol. Vis. Sci. 57 (6) (2016) 2864–2875.
[28] M. Mesquida, et al., Modelling macular edema: the effect of IL-6 and IL-6R blockade on human blood-retinal barrier integrity in vitro, Transl Vis Sci Technol 8 (5) (2019) 32.
[29] E.G. Sergeeva, et al., Neurosteroid allopregnanolone reduces ipsilateral visual cortex potentiation following unilateral optic nerve injury, Exp. Neurol. 306 (2018) 138–148.
[30] L. He, et al., HOXA9 gene inhibits proliferation and differentiation and promotes apoptosis of bovine preadipocytes, BMC Genom. 25 (1) (2024) 358.
[31] M. Kaufmann, Z. Han, RPE melanin and its influence on the progression of AMD, Ageing Res. Rev. 99 (2024) 102358.
[32] H. He, et al., Glycyrrhizin protects against sodium iodate-induced RPE and retinal injury though activation of AKT and Nrf2/HO-1 pathway, J. Cell Mol. Med. 23 (5) (2019) 3495–3504.
[33] Y.Y. Chang, et al., Protective effect of quercetin on sodium iodate-induced retinal apoptosis through the reactive oxygen species-mediated mitochondrion-dependent pathway, Int. J. Mol. Sci. 22 (8) (2021).
[34] J. Zhao, H.J. Kim, J.R. Sparrow, Multimodal fundus imaging of sodium iodate-treated mice informs RPE susceptibility and origins of increased fundus autofluorescence, Invest. Ophthalmol. Vis. Sci. 58 (4) (2017) 2152–2159.
[35] D. Guo, et al., IGF2 inhibits hippocampal over-activated microglia and alleviates depression-like behavior in LPS- treated male mice, Brain Res. Bull. 194 (2023) 1–12.
[36] A. Proces, et al., Stretch-injury promotes microglia activation with enhanced phagocytic and synaptic stripping activities, Biomaterials 305 (2024) 122426.
[37] J.N. Dai, et al., Gastrodin inhibits expression of inducible NO synthase, cyclooxygenase-2 and proinflammatory cytokines in cultured LPS-stimulated microglia via MAPK pathways, PLoS One 6 (7) (2011) e21891.
[38] J.E. Yuste, et al., Implications of glial nitric oxide in neurodegenerative diseases, Front. Cell. Neurosci. 9 (2015) 322.
[39] Y. Wang, et al., The role of IL-1beta and TNF-alpha in intervertebral disc degeneration, Biomed. Pharmacother. 131 (2020) 110660.
[40] Y. Dou, et al., Microglial migration mediated by ATP-induced ATP release from lysosomes, Cell Res. 22 (6) (2012) 1022–1033.
[41] D. Fisch, et al., Molecular definition of the endogenous Toll-like receptor signalling pathways, Nature 631 (8021) (2024) 635–644.
[42] X. Fei, et al., The Scap-SREBP1-S1P/S2P lipogenesis signal orchestrates the homeostasis and spatiotemporal activation of NF-kappaB, Cell Rep. 42 (6) (2023) 112586.

[43] H. Ma, F. Yang, X.Q. Ding, Inhibition of thyroid hormone signaling protects retinal pigment epithelium and photoreceptors from cell death in a mouse model of age-related macular degeneration, Cell Death Dis. 11 (1) (2020) 24.
[44] N. Pankova, et al., Evolving patterns of hyperfluorescent fundus autofluorescence accompany retinal atrophy in the rat and mimic atrophic age-related macular degeneration, Transl Vis Sci Technol 11 (3) (2022) 3.
[45] P.S. Tate, et al., Ilex paraguariensis extracts prevent oxidative damage in a mouse model of age-related macular degeneration, Mol. Nutr. Food Res. 66 (10) (2022) e2100807.
[46] B. Yang, Y. Chen, J. Shi, Reactive oxygen species (ROS)-Based nanomedicine, Chem Rev 119 (8) (2019) 4881–4985.
[47] F.Y.F.H. Li, Dual detoxification and inflammatory regulation by ceria nanozymes for drug-induced liver injury therapy, Nano Today 1 (35) (2020).
[48] V. Enzmann, et al., Behavioral and anatomical abnormalities in a sodium iodate-induced model of retinal pigment epithelium degeneration, Exp. Eye Res. 82 (3) (2006) 441–448.
[49] L.M. Franco, et al., Decreased visual function after patchy loss of retinal pigment epithelium induced by low-dose sodium iodate, Invest. Ophthalmol. Vis. Sci. 50 (8) (2009) 4004–4010.
[50] G.T. Prusky, et al., Rapid quantification of adult and developing mouse spatial vision using a virtual optomotor system, Invest. Ophthalmol. Vis. Sci. 45 (12) (2004) 4611–4616.